MAGMATIC HYDROTHERMAL FLUIDS AND THE ORIGIN OF QUARTZ – TOURMALINE ORBICULES IN THE SEAGULL BATHOLITH, YUKON TERRITORY*

IAIN M. SAMSON

Department of Geology, University of Windsor, Windsor, Ontario N9B 3P4

W. DAVID SINCLAIR

Geological Survey of Canada, 601 Booth Street, Ottawa, Ontario K1A OE8

ABSTRACT

The mid-Cretaceous Seagull batholith in the Yukon Territory consists of meta- to peraluminous granite in which tourmaline generally occurs as an accessory phase. The roof zone of the granite is, however, characterized by the presence of quartz–tourmaline orbicules that constitute up to 10 to 15% of the granite. The orbicules are typically 6 to 8 cm in diameter, and contain up to 40% tourmaline, the remainder being chiefly quartz, feldspar, and minor fluorite. Miarolitic cavities lined with quartz, tourmaline, and rare topaz occur in the center of some orbicules. The orbicules crystallized from a mixture of residual borosilicate melt and hydrothermal fluid. Quartz, tourmaline and fluorite contain primary aqueous fluid inclusions. Salinities range from 8 to 42 equiv. wt.% $NaCl + CaCl_2$. As the orbicules crystallized as closed systems, these inclusions contain unevolved orthomagmatic hydrothermal fluids. Large variations in salinity of fluids associated with epizonal plutons thus do not have to be explained by boiling or mixing with meteoric water. Isochoric projections indicate that crystallization took place between 600 and 300°C, and possibly as low as 150°C. Solids associated with some of these inclusions demonstrate that the fluids were in equilibrium with muscovite, indicating that they would cause phyllic alteration during migration through previously crystallized granite. Elevated concentrations of tin in the orbicules and the presence of quartz–tourmaline–cassiterite veins in the granite indicate that, on occasion, the fluids migrated away from the magma and were responsible for the tin mineralization associated with the granite.

Keywords: magmatic hydrothermal fluid, granite, quartz–tourmaline orbicules, tin mineralization, Seagull batholith, Yukon.

SOMMAIRE

Le batholite de Seagull, situé dans le Territoire du Yukon, et d'âge crétacé moyen, est formé d'un granite méta-à hyperalumineux dans lequel la tourmaline forme en général une phase accessoire. Cependant, dans la coupole, des orbicules à quartz + tourmaline peuvent constituer jusqu'à 10-15% du granite. Les orbicules ont typiquement 6 à 8 cm de diamètre et contiennent jusqu'à 40% de tourmaline, le reste étant constitué essentiellement de quartz, feldspath et fluorite en quantité mineure. Des cavités miarolitiques, renfermant quartz, tourmaline, fluorite en quantité mineure et rare topaze, existent au centre de certaines orbicules. Les orbicules se sont formées à partir d'un mélange de magma résiduel borosilicaté et de fluide hydrothermal. Quartz, tourmaline et fluorite contiennent des inclusions fluides aqueuses primaires, avec des salinités allant de 8 à 42% équivalents en poids de $NaCl + CaCl_2$. Les orbicules ont cristallisé en système fermé; ces inclusions contiennent donc un échantillon de la phase fluide orthomagmatique non évoluée. Les variations importantes en salinité qui caractérisent les plutons épizonaux ne nécessitent donc pas une explication faisant appel à une ébullition ou à un mélange avec de l'eau météorique. Les projections isochores indiquent une cristallisation entre 600 et 300°C, et même peut être jusqu'à 150°C. En outre, les inclusions solides associées montrent que dans certains cas, le fluide était en équilibre avec la muscovite, ce qui fait penser qu'il pourrait causer une altération phyllique s'il traversait le granite cristallisé. La richesse en étain des orbicules et la présence dans le granite de fissures remplies de quartz + tourmaline + cassitérite montrent que ce fluide a pu parfois migrer en dehors du magma et induire la minéralisation en étain associée au granite.

(Traduit par la Rédaction)

Mots-clés: fluide hydrothermal orthomagmatique, granite, orbicules à quartz + tourmaline, minéralisation en étain, batholite de Seagull, Yukon.

INTRODUCTION

The roof zone of the mid-Cretaceous Seagull batholith, located near the southern border of the Yukon Territory, is characterized by the presence of quartz–tourmaline orbicules. These have been attributed to a borosilicate fluid transitional in composition between silicate melt and hydrother- mal fluid, that evolved during the late stages of crystallization of the granite (Sinclair & Richardson 1992). Elevated tin concentrations (up to 90 ppm) in the orbicules suggest that these late-stage fiuids also were responsible for the tin mineralization in and around the batholith. This paper communi- cates the results of a study of fluid inclusions initiated in order to characterize the fluids from
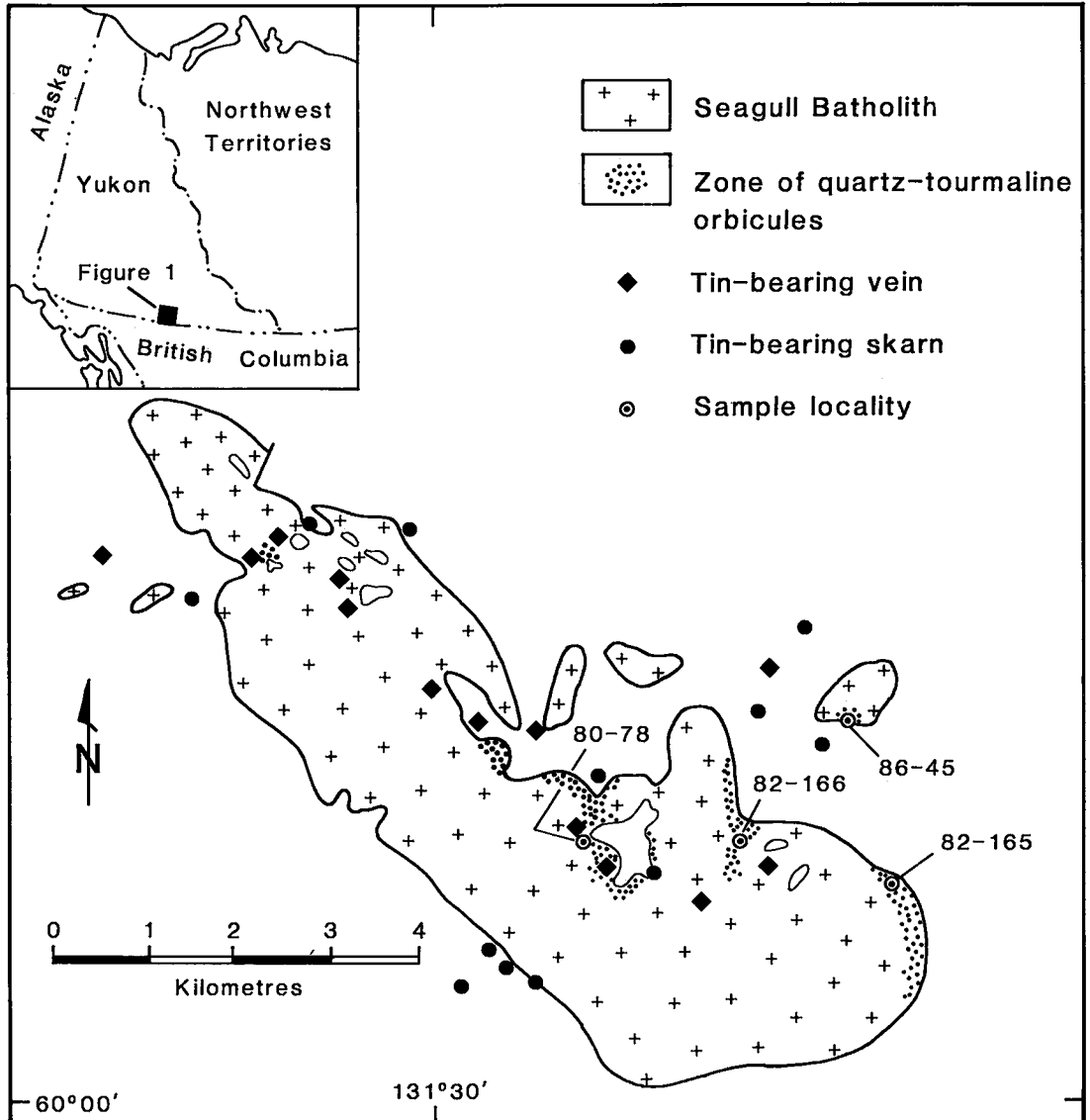

FIG. 1. Distribution of quartz–tourmaline orbicules and tin-bearing veins and skarns associated with the Seagull batholith, Yukon Territory. Modified from Mato *et al.* (1983) and Sinclair (1986).

which the orbicules crystallized, to elucidate their origin, and to provide information on any orthomagmatic hydrothermal fluids that may have played a role in tin mineralization.

GEOLOGY

The Seagull batholith (Fig. 1), which hosts the quartz–tourmaline orbicules, is a leucocratic granite of mid-Cretaceous age (Mato et al. 1983), exposed over about 300 km^2 in the Cassiar Mountains in southeastern Yukon Territory. It was emplaced in the Yukon Cataclastic Complex, a tectonic mélange of sedimentary, volcanic and intrusive rocks deformed during the Early Mesozoic collision between the ancient North American craton and an allochthonous island arc terrane (Tempelman-Kluit 1979, Abbott 1981). The batholith has a high initial $^{87}Sr/^{86}Sr$ value of 0.712 (Mato et al. 1983) and likely crystallized from a magma derived by partial melting of crustal rocks related to the Early Mesozoic collision.

Mineralogical and chemical aspects of the Seagull batholith have been described by Gower (1952), Poole (1956), Mato et al. (1983) and Sinclair & Richardson (1992). The batholith consists entirely of leucocratic granite; medium- to coarse-grained seriate granite forms approximately 90% of the exposures, and fine-grained, commonly porphyritic granite, about 10%. The coarser-grained seriate granite occurs mainly in the central part of the batholith, whereas the finer-grained porphyritic granite is more common near the margin. Contacts between the two varieties are typically irregular and gradational. The two varieties of granite are similar mineralogically, and average 38% quartz, 33% K-feldspar, 25% plagioclase and 4% biotite. Accessory minerals include fluorite (0.5–1%) and trace amounts of ilmenite, rutile, monazite and topaz.

A relatively shallow level of emplacement of the granite (1 < P < 2 kbar?) is indicated by sharp contacts with country rocks, the presence of miarolitic cavities, and the fine-grained, porphyritic texture of the granite near its margin.

Chemical compositions presented by Mato et al. (1983) and Sinclair & Richardson (1992) show that the Seagull granite is slightly metaluminous to peraluminous (all compositions are characterized by normative corundum), siliceous (74–77% SiO_2), alkali-rich (8–9% $K_2O + Na_2O$), rich in fluorine (0.15–0.65% F) and poor in TiO_2 (0.09–0.13%), Fe_2O_3 (0.1–0.4%), FeO (0.6–1.2%), CaO (0.39–0.71%) and MgO (0.01–0.18%). The Seagull granite also has relatively high contents of lithophile elements such as Li (36–176 ppm), Be (6.1–14 ppm), Nb (57–77 ppm), Y (87–220 ppm), Rb (326–668 ppm) and Ga (23.3–27.4 ppm), but only minor Ba (30–124 ppm) and Sr (9–28 ppm), compared to average granitic rocks. The chemical composition of the Seagull granite is typical of highly differentiated, "specialized" granites (cf. Tischendorf 1977).

Although the tin content of the Seagull granite (< 3–10 ppm Sn) is not anomalous, tin-bearing veins and skarns are associated with the batholith and probably are genetically related (Fig. 1). Aspects of the tin deposits have been described by
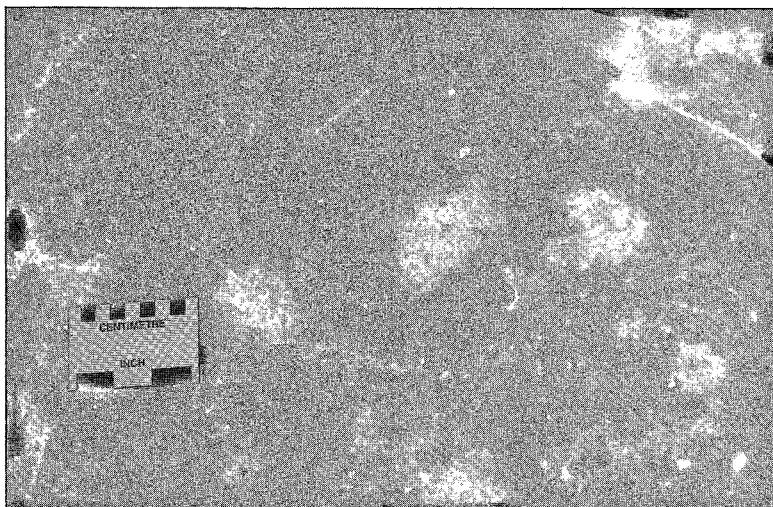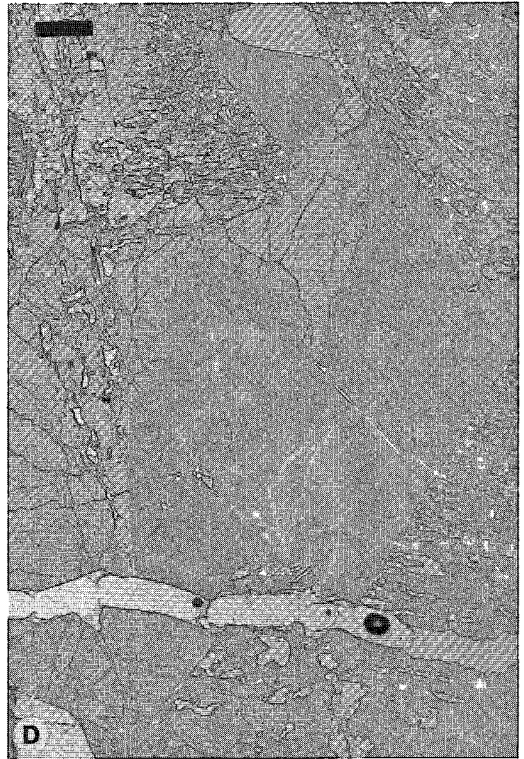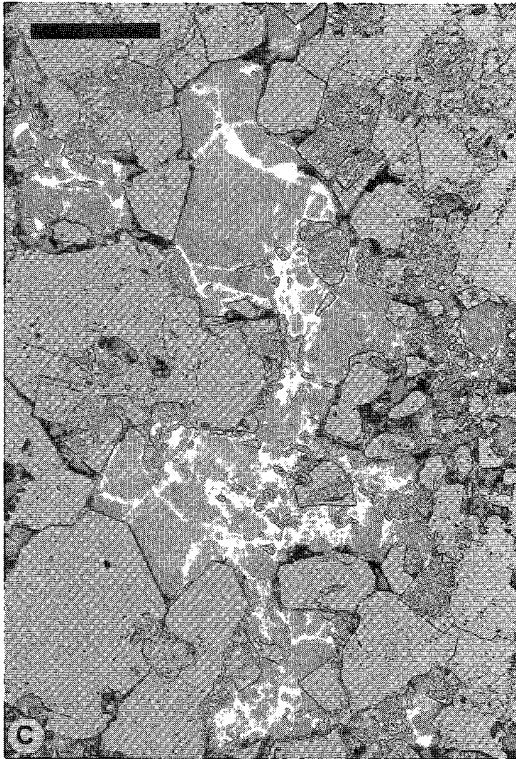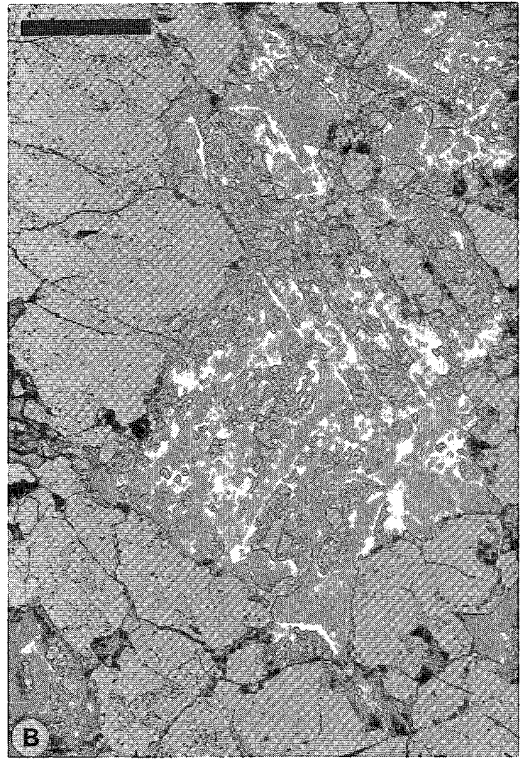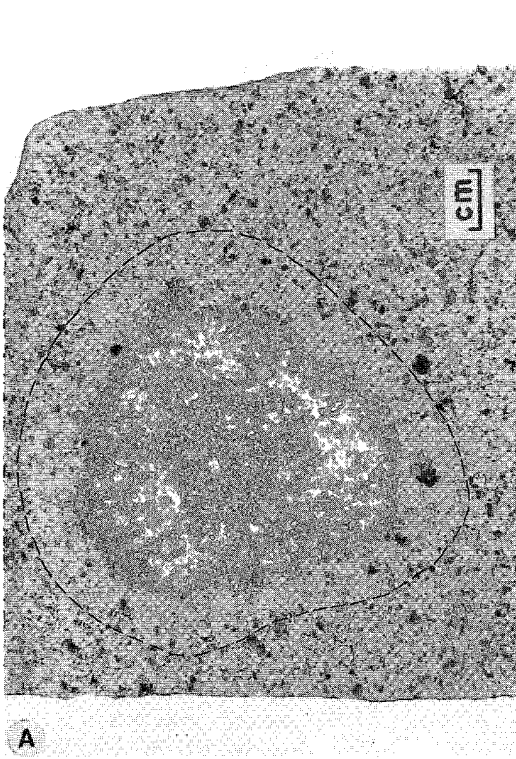

FIG. 2. Quartz–tourmaline orbicules in the Seagull granite.

Dick (1980), Mato *et al.* (1983), Layne & Spooner (1986, 1991) and Sinclair (1986).

Except in the highest levels of the exposed batholith, the Seagull granite generally contains only trace amounts of tourmaline. The upper part of the batholith, however, contains orbicules that are characterized by abundant tourmaline and quartz (Fig. 2). The orbicules are roughly spherical to ovoid in shape (Fig. 3A), but may be joined in places to form larger, more irregular bodies. Spherical orbicules are typically 6 to 8 cm in diameter, but range from 2 to 10 cm or more. Tourmaline-bearing fractures and quartz–tourmaline veins also are present in the upper part of the batholith. Some orbicules are cut by tourmaline-bearing veins, but most orbicules are spatially unrelated to such features. The orbicules and veins occur in both the seriate and fine-grained granites.

The orbicules are concentrated at the top of the batholith, where they constitute, in places, 10 to 15% of the granite. They extend to several hundred meters below the upper contact, gradually decreasing in abundance with depth. They are most abundant in the southeastern exposures of the batholith, particularly along the eastern and northeastern margins and beneath roof pendants (Fig. 1).

MINERALOGY

The orbicules consist mainly of tourmaline and quartz, with lesser amounts of microcline, albite and minor amounts of fluorite. They commonly exhibit concentric zonation based on the proportion of the constituent minerals (Fig. 3A). From host granite inward, this zonation consists of a leucocratic halo of biotite-free granite 1 to 2 cm wide that surrounds each orbicule, a dark outer zone 1 to 5 cm wide that consists mainly of quartz and tourmaline, and a slightly more leucocratic inner zone with a radius of 1 to 2 cm and composed of quartz, microcline, albite and tourmaline. In many orbicules, the dark outer zone extends to the center of the orbicule, and the leucocratic inner zone is absent. Some orbicules have a central

miarolitic cavity lined with crystals of quartz, tourmaline and, in a few places, topaz.

The leucocratic halo that surrounds each orbicule consists of host granite that is characterized by the absence of biotite. The lack of any obvious alteration-related features suggests that the absence of biotite is a primary feature and is not due to alteration of pre-existing biotite.

The transition from the leucocratic halo to the dark outer zone is marked by the abrupt appearance of dark brown to black tourmaline, which constitutes 25 to 40% of the zone (by volume). The tourmaline is generally fine grained and anhedral. Quartz (35–50%), albite (10–30%) and perthitic microcline (0–15%) are the other principal minerals. Minor amounts of fluorite (0–1%) and trace amounts of muscovite, rutile, zircon, thorite, ilmenite, pyrite, arsenopyrite, wolframite, monazite and topaz also are present. Tin in the orbicules is principally concentrated in rutile (Sinclair & Richardson 1992).

An examination of thin sections shows that the tourmaline in the outer zone has replaced microcline, albite and quartz to varying degrees. Incipient stages of tourmalinization consist of stringers and irregular networks of tourmaline partly replacing perthitic microcline (Fig. 3B). Advanced stages of this alteration are characterized by nearly complete to complete replacement of microcline and associated albite intergrowths, partial replacement of discrete albite grains, and replacement of quartz along grain boundaries. Tourmaline replacing microcline commonly contains inclusions of quartz and remnants of microcline and albite. Rutile, zircon, thorite and monazite also occur as inclusions in tourmaline. In some orbicules, minor amounts of muscovite occur as an alteration product of microcline, particularly in association with tourmaline, and in cases interstitially to quartz, feldspar and tourmaline.

The more leucocratic inner zone of the orbicules consists of fine-grained quartz (30–40%), tourmaline (20–40%), microcline (20–25%), albite (15–20%) and fluorite (0.5–1%). In this zone, tourmaline typically occurs as discrete, anhedral, interstitial grains that generally show no evidence of replacement of the feldspars (Figs. 3C,D).

FIG. 3. A. Quartz–tourmaline orbicule showing the leucocratic halo in granite (outlined by dashed line), dark outer zone, and slightly more leucocratic inner zone. B. Photomicrograph showing K-feldspar partly replaced by tourmaline (dark grey), albite relatively unreplaced, and quartz. C. Photomicrograph showing tourmaline, in part replacing K-feldspar (cloudy grains) and in part infilling cavity (note euhedral terminations on quartz grains projecting into tourmaline). D. Photomicrograph of zoned tourmaline in core of orbicule; tourmaline fills cavity bounded by K-feldspar, which is extensively replaced by tourmaline. Scale bar = 0.5 mm.
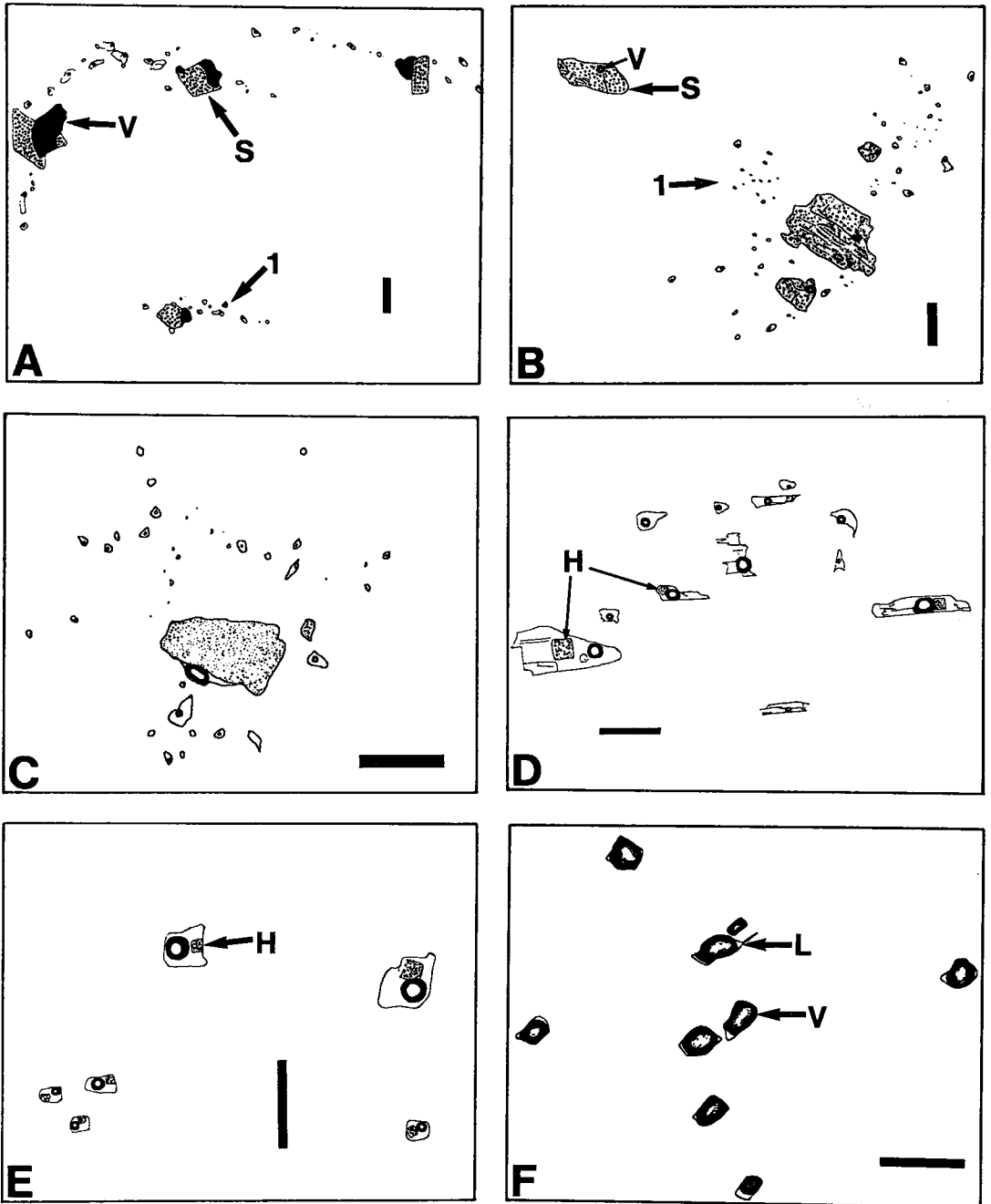
FIG. 4. Drawings of fluid inclusions from the quartz–tourmaline orbicules. A. Growth zone in quartz containing type-1 and type-6 inclusions with unknown rhombic solid. B. Type-6 inclusions (muscovite) with and without arrays of type-1 inclusions. C. Isolated array of type-6 inclusion (muscovite) surrounded by a cluster of type-1 inclusions. D. Primary type-1 and type-5 inclusions in tourmaline. E. Primary type-5 inclusions in quartz. F. Secondary type-3 inclusions in quartz. 1, type-1 inclusion; L, liquid; V, vapor; S, solid; H, halite. Scale bar = 20 μm.

Tourmaline also occurs, less commonly, as irregular grains within granophyric intergrowths of quartz and K-feldspar.

Representative orbicules from four different localities in the Seagull batholith were used in this study (Fig. 1).

ANALYTICAL TECHNIQUES

Microthermometric analyses were carried out on a Linkam TH600 heating–freezing stage calibrated with various organic and inorganic liquids and solids, H_2O and melting-point standards. Raman spectra were collected at the University of Windsor on an Instruments S.A., Ramanor U-1000 spectrometer fitted with a Spectra Physics Ar ion laser (514.5 nm line) and a Nachet microscope (X80 objective), using a counting time of 1 second and a stepping interval of 1 cm^{-1}.

TYPES OF FLUID INCLUSIONS

In the orbicules, fluid inclusions are present in quartz, tourmaline, and fluorite. Inclusions appear to be less abundant in tourmaline than in quartz; however, inclusions in tourmaline are generally obscured by the dark color and high indices of refraction of the host. Fluorite is rare in the samples studied; inclusions were only observed in fluorite from sample 80–78.

Six types of fluid inclusions are present in these minerals (Fig. 4), distinguished on the basis of ratio of included phases at room temperature. Generally, only groups of inclusions with apparently consistent ratios of phases have been described and measured. Measurements on trapped phases were not attempted. All results are reported as the average and standard deviation for a single, cogenetic group, except in those cases where analytical difficulties allowed only one result to be obtained from a group, or the rare situation where a single, isolated inclusion was measured. The six types of inclusion are:

1. Two-phase, liquid–vapor aqueous inclusions (Fig. 4C) that homogenize to the liquid phase. These inclusions may contain trapped, generally birefringent, solids.

2. One-phase, liquid-only aqueous inclusions. These are generally associated with type-1 inclusions with high degrees of fill, and either represent the same fluid in which a vapor bubble has failed to nucleate, or part of a necked inclusion.

3. Two-phase, vapor–liquid (vapor-rich) inclusions (Fig. 4F).

4. One-phase, vapor-only inclusions.

5. Aqueous liquid–vapor–solid inclusions. In a majority of these inclusions, the only daughter mineral present is a subhedral to euhedral square (cubic) solid, interpreted as halite (see later section) (Fig. 4E). Some inclusions contain additional solids, which, in most cases, are small and not present in all inclusions (trapped). In some, rare, secondary groups, these additional solids are large, are present in all inclusions in a group, and therefore may be daughter minerals.

6. Generally large (20 – 100 μm), solid ± vapor ± liquid inclusions. In most inclusions, the solids exhibit strong birefringence and can be anhedral or euhedral. The vapor phase varies from a small sphere to a large irregular mass (Figs. 4A, B, C). In a few examples, these inclusions contain two vapor bubbles, one on either side of the solid (Fig. 5E). In some inclusions, a volumetrically minor liquid phase may is present.

Primary inclusions

Primary inclusions in quartz occur in a variety of forms: in growth zones, as small, isolated clusters, and as dispersed, three-dimensional arrays. Growth zones may comprise type-6, type-1, or a mixture of both types of inclusion (Fig. 4A). Large, isolated, type-6 inclusions are common and are also interpreted as primary (Fig. 4B).

Isolated type-6 inclusions commonly have an array of small inclusions associated with them (Figs. 4B, C, 5E). These arrays generally comprise type-1, with or without type-2, inclusions; one array contains type-5 inclusions. The arrays are, in most cases, isolated from other groups of inclusions: some crystals have numerous, large, type-6 inclusions, each with their own envelope of type-1 inclusions. Most of the arrays appear to be planar, although some are distributed around the central type-6 inclusion in a three-dimensional cluster. In rare cases, several large type-6 inclusions may lie within a single type-1 array. In many crystals, type-1 inclusions are only found associated with type-6 inclusions. It is clear that there is a genetic link between the type-6 inclusions and the associated type-1 arrays. The arrays could represent: 1) pseudosecondary planes, 2) decrepitation clusters, or 3) growth surfaces, where the type-1 inclusions were trapped at the same time as the type-6 inclusions. If the arrays represent pseudosecondary planes, the solid (type-6 inclusion) would have to have been precipitated in the fracture, as most are probably too large (commonly 50 to 100 μm) to have been trapped along with the fluid. In such a model, it is difficult to explain why the solid always occurs at, or close to, the center of the array. We therefore do not consider these to be pseudosecondary inclusions.

Planar arrays of small inclusions around a larger central inclusion may also be produced through decrepitation as a result of internal overpressure
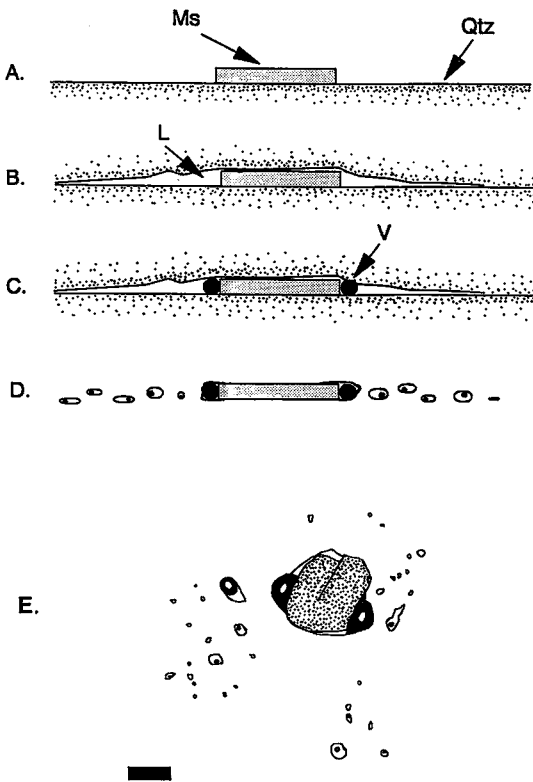
FIG. 5. A to D. Sequence of sketches illustrating a proposed model for the formation of the 1/6 arrays of fluid inclusions on a growth surface of quartz (Qtz), as induced by the precipitation of muscovite (Ms) (or any other mineral). This sketch includes the formation of two vapor bubbles on either side of the muscovite crystal. E. Drawing of an actual 1/6 array showing two vapor bubbles in the type-6 inclusion. Scale bar = 10 μm.

negative crystals, and the arrays are not always restricted to the immediate vicinity of the type-6 inclusions, both of which would argue against an origin through decrepitation. Therefore, we interpret these arrays to be primary growth-related features, analogous to the growth zones in Figure 4A, but where inclusions have formed over a more restricted part of the growth surface. Note that each section of the growth zone in Figure 4A comprises a type-6 inclusion surrounded by type-1 inclusions. In this interpretation, the solid is central to the formation of the type-1 array, both literally and figuratively. Our interpretation is that the solid, precipitated on the surface of the growing quartz crystal, acted as a discontinuity in the growth of the quartz. This resulted in the trapping of some fluid in a restricted growth-zone immediately around the solid, which subsequently healed to form a planar to three-dimensional array of type-1 and type-2 inclusions, with a type-6 inclusion at its center (Fig. 5A–D). Isolation of fluid on either side of the solid and subsequent healing also explain the presence of two vapor bubbles, on opposite sides of the solid, in some type-6 inclusions (Fig. 5B).

In sample 80–78, primary type-5 inclusions occur as a a three-dimensional array (Fig. 4E). This sample is free of any other type of primary inclusions.

Many tourmaline crystals contain abundant elongate or tubular inclusions that are aligned parallel to the Z axis of the crystal; these are interpreted as primary inclusions (Fig. 4D). The contents of these inclusions, particularly the solid phases, are commonly difficult to resolve optically owing to the color and indices of refraction of the tourmaline. These inclusions are either type-1 or type-5. Some crystals appear to have mixtures of the two types of inclusion (Fig. 4D), but this may be a problem in resolving halite in these dark inclusions.

The only inclusions in fluorite that may be primary are large, isolated, type-5 inclusions in sample 80–78.

Pseudosecondary inclusions

Type-1 and type-5 inclusions that form short, isolated planes have been interpreted as pseudosecondary, although, by analogy with the arrays discussed above, they could represent surfaces of restricted growth that formed without the aid of a solid.

Secondary inclusions

Secondary planes are common in all samples and contain all the types of inclusion described, with the exception of type 6. Inclusions of types 3 and

exerted by the central inclusion (Pécher 1981, Sterner & Bodnar 1989). Inclusions that re-equilibrate to a lower external pressure tend to become negative crystals (Gratier & Jenatton 1984, Sterner & Bodnar 1989), and may also decrepitate to form a plane of uniformly small inclusions immediately surrounding the original inclusion (Pécher 1981). Sterner & Bodnar (1989) have, however, cast some doubt on the frequency with which decrepitation clusters form. In their experiments, they found that the formation of a decrepitation cluster was "the rare exception rather than the rule" (p. 251), and suggested that many of the arrays described by other investigators from experimental studies may in fact be unrelated to decrepitation.

The central inclusions in the Seagull arrays of inclusions tend to be irregularly shaped, rather than

TABLE 1. SUMMARY OF THERMOMETRY DATA FOR INCLUSION TYPES 1 AND 6

SAMP	MIN	TYPE	ORIG	#	Te ave	s.d.	TmICE ave	s.d.	SAL	TdV ave	s.d.
78	F	1	?	2	-34.0	-	-4.1	0.0	7.1	233	25
78	F	1	S	3	-35.0	-	-5.3	0.0	8.7	260	4
78	F	1	S	2	-	-	-4.3	0.1	7.3	276	1
78	F	1	S	1	-	-	-3.3	-	5.9	160	10
165a	Q	1	?	3	-45.0	-	-23.0	-	22.7	75	1
78	Q	1	?	5	-27.0	-	-5.0	3.3	8.3	-	-
166c	Q	1	?	1	-	-	-	-	-	140	-
45a	Q	1	P1	8	-34.0	1.4	-8.6	0.3	12.7	126	22
45a	Q	1	P1?	1	-35.0	-	-14.9	-	18.2	312	-
45a	Q	1	P1?	5	-	-	-10.3	0.0	14.4	378	18
78	Q	1	PS	6	-23.0	4.0	-15.3	0.1	18.5	226	65
78	Q	1	PS	1	-35.0	-	-13.9	-	17.5	-	-
45a	Q	1	PS/S	2	-40.0	-	-8.8	-	12.9	97	0
45a	Q	1	S	4	-	-	-8.6	0.4	12.7	375	7
45a	Q	1	S	2	-35.0	-	-8.8	-	12.9	113	4
45a	Q	1	S	4	-40.0	0.0	-8.3	0.7	12.4	116	11
166c	Q	1	S	2	-25.0	-	-2.7	0.0	4.9	-	-
45a	Q	1	S	4	-25.0	8.6	-8.3	0.3	12.4	130	5
45a	Q	1	S	4	-25.0	0.0	-8.2	0.2	12.3	145	13
165a	Q	1	S	6	-40.0	-	-3.7	0.0	6.5	123	10
45c	Q	1	S	2	-	-	-7.1	0.2	11.0	-	-
78	Q	1	S	2	-	-	-3.3	-	5.9	285	41
165a	Q	1	S	3	-	-	-3.7	-	6.5	133	4
45a	Q	1	S	6	-35.0	0.0	-8.8	0.1	12.9	136	25
45c	Q	1	S	5	-47.0	-	-7.1	0.0	11.0	122	11
78	Q	1	S	4	-	-	-2.8	0.4	5.1	153	22
166b	T	1	P5	2	-	-	-4.5	-	7.6	111	2.0
45b	T	1	P5	5	-27.0	-	-20.0	1.0	21.3	143	12.0
45b	T	1	P5	1	-	-	-11.0	-	15.1	260	-
165a	Q	1(1S)	P2/PS	4	-45.0	-	-16.0	-	19.0	87	2
45a	Q	1(6)	?	5	-	-	-7.7	0.3	11.7	-	-
166b	Q	1(6)	P1	5	-	-	-9.5	0.0	13.6	110	10
45c	Q	1(6)	P3	7	<-40	-	-5.8	1.0	9.3	126	30
166c	Q	1(6)	P6	7	-50.0	-	-13.7	0.4	17.3	127	13
166c	Q	1(6)	P6	1	-50.0	-	-10.8	-	14.9	198	-
165a	Q	1(6)	P6	1	<-40	-	-22.0	-	22.2	-	-
165a	Q	1(6)	P6	2	-	-	-	-	0.3	101	1
166c	Q	1(6)	P6	1	-	-	-11.0	-	15.1	-	-
45a	Q	1(6)	P6	3	-	-	-5.0	0.2	8.3	181	15
165a	Q	1(6)	P6	3	-	-	-8.2	-	12.3	114	23
166c	Q	1(6)	P6	2	-50.0	-	-18.5	0.7	20.5	140	8
165a	Q	1(6)	P6?	3	-	-	-	-	0.3	127	16
165a	Q	1(6)	PS/P3	6	-40.0	-	-10.4	0.4	14.5	115	13
45c	Q	1(6)	PS/P3?	4	-35.0	-	-7.5	0.2	11.5	114	13
165a	Q	1(6?)	P6?	2	<-30	-	-12.2	0.0	16.1	127	2
78	Q	1/1S	?	3	-25.0	-	-20.5	0.6	21.5	175	59
166c	Q	1/2	S?	2	-	-	-	-	-	124	19
166c	Q	1/6	P6	2	-	-	-23.0	3.0	22.7	-	-
78	Q	1S	?	1	-37.0	-	-25.0	-	23.5	-	-
78	Q	1S/1	?	1	-26.0	-	-23.2	-	22.7	-	-
45a	Q	1b	S	12	-30.0	-	-9.3	0.5	13.4	356	3
165a	Q	1s	PS/P2	2	-50.0	-	-25.0	0.0	23.5	77	7
45c	Q	6	P2	3	-	-	-7.6	-	11.5	370	49
45c	Q	6	P3	1	-	-	-7.7	-	11.7	384	-

MIN: Mineral: Q, Quartz; F, Fluorite; T, Tourmaline
TYPE: Type of inclusion as defined in text (phase assemblage)
ORIG: Origin of inclusion group: P, Primary (P1, growth zone;
    P2, 3D array; P3, 1/6 array; P4, isolated incl.; P5, tubular incl in
    tourmaline); PS, Pseudosecondary; S, Secondary
#: Number of inclusions in group used for averages (ave.) and
    standard deviation (s.d.)
SAL: Salinity in equiv. wt. % NaCl + CaCl2
All temperature measurements in degrees C

4 were found only along secondary planes (Fig. 4F).

COMPOSITIONS OF INCLUSIONS AND PHASE BEHAVIOR

Tables 1, 2 and 3 contain a summary of the microthermometric results obtained on the fluid inclusions. Results are given as the average value for a cogenetic group, along with the standard deviation for that group. Data points on diagrams also represent average values.

Type-1 inclusions

Type-1 inclusions homogenize to the liquid phase

TABLE 2. SUMMARY OF THERMOMETRY DATA FOR INCLUSION TYPES 3 AND 4

SAMP	MIN	TYPE	ORIG	#	TmCO2		TmCTH	ThP		ThT
					ave	s.d.	ave	ave	s.d.	
45a	Q	4	S	2	-59.0	-	-	-	-	-
166c	Q	3	S	3	-58.3	0.1	-	-	-	360-420
166c	Q	3	S	5	-58.2	0.2	6	-1.1	0.7	390-410
78	Q	3/4	S?	2	-58.3	-	-7	-	-	-
78	Q	3	S	1	-59.2	-	5-8	-	-	-
166d	Q	3	S	5	-58.8	0.1	5	4	-	350-450

ThT: Total homogenization of the inclusion

TABLE 3. SUMMARY OF THERMOMETRY DATA FOR INCLUSION TYPE 5

SAMP	MIN	TYPE	ORIG	#	Te		TmICE		SAL	TdV		Td HALITE	
					ave	s.d.	ave	s.d.		ave	s.d.	ave	s.d.
78	F	5	P4	2	-65.0	-	-32.0	0.6	35.1	435	7	200	7
78	Q	5	P2	4	-46.0	-	-28.0	-	41.6	268	38	284	31
78	Q	5	PS/P	5	-	-	-	-	-	140	44	220	88
78	Q	5	PS?	4	-	-	-	-	-	232	4	216	5
78	Q	5	PS?	3	-92.0	-	-39.4	3.0	47.5	131	-	350	5
78	Q	5	S	3	-	-	-	-	-	240	21	247	20
78	Q	5	S	2	-81.0	-	-	-	-	183	-	nc500	-
78	Q	5	S	2	-65.0	-	-35.8	6.0	34.3	95	3	165	28
78	Q	5	S	8	-75.0	-	-49.5	1.5	48.9	188	16	357	18
78	Q	5	S	3	-88.0	15.0	-	-	-	222	72	452	114
78	Q	5	S	7	-65.0	-	-36.5	2.0	52.2	190	25	410	28
78	Q	5	S	9	-65.0	-	-36.5	2.0	44.9	207	16	311	21
78	Q	5	S	3	-78.0	5.0	-54.2	5.4	51.3	141	3	393	45
166b	T	5	?	1	-60.0	-	-29.6	-	43.5	>450?	-	304	-
78	T	5	P4	1	-65.0	-	-	-	-	-	-	-	-
78	T	5	P5	1	-65.0	-	-37.7	-	-	-	-	-	-
78	T	5	P5	1	-86.0	-	-43.0	-	39.2	306	-	230	-
165a	T	5	P5	1	-	-	-	-	-	480	-	327	-
78	T	5	P5	5	-60.0	-	-32.0	-	38.0	301	26	232	6
166c	Q	5(6)	P1	6	-67.0	-	-27.1	0.4	37.5	108	21	220	28

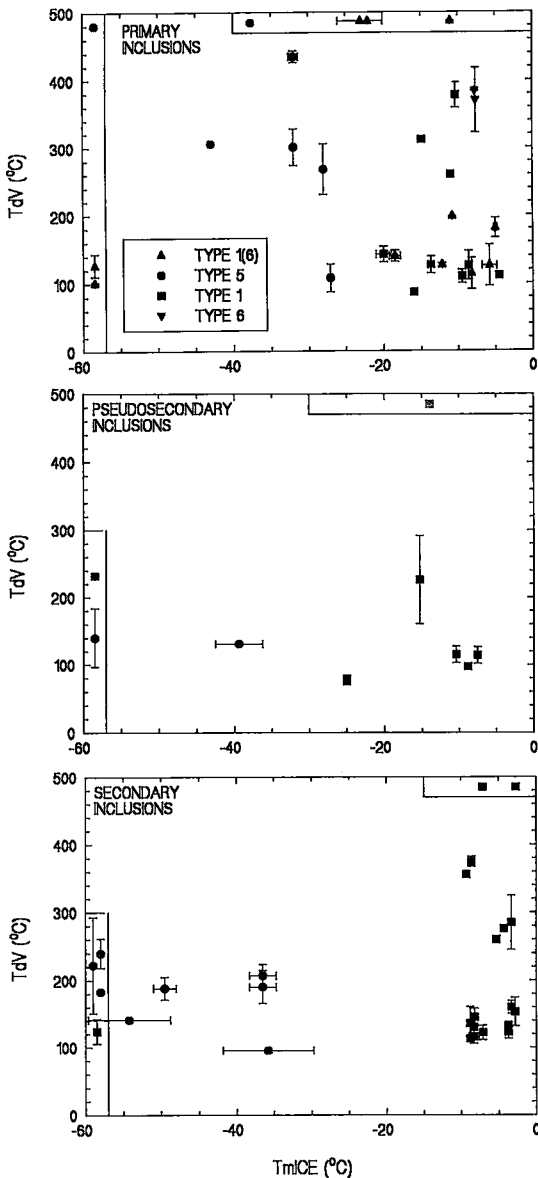**nc: No change in the solid at the indicated temperature**

FIG. 6. Temperatures of vapor disappearance and ice melting for type-1, type-5 and type-6 primary, pseudo-secondary and secondary inclusions. Type 1(6) are those type-1 inclusions associated with a type-6 inclusion (Figs. 4B, C, 5E). For type-1 inclusions, TdV is the temperatures of homogenization. Each point represents the average for a cogenetic group. Error bars represent standard deviations for each group. Points in boxes adjacent to top and left-hand axes represent groups of inclusions where either TmICE or TdV is known.

at temperatures of between 69 and 392°C. Eutectic temperatures (Te) were generally found to be difficult to measure, but where observed, range from −50 to −20°C. Final melting of ice (TmICE) occurred between −25 and −2.7°C (Fig. 6). Because of the low eutectic values and TmICE values below −20.8°C, salinities have been calculated in terms of the system $H_2O–NaCl–CaCl_2$ and represent the median salinity for a given TmICE in that system (Oakes *et al.* 1990).

Primary and pseudosecondary inclusions have overall lower TmICE values (higher salinities) than secondary inclusions; salinities of primary and pseudosecondary type-1 inclusions range from 6.6 to 24.3 equiv. wt.% NaCl + $CaCl_2$. There are no secondary inclusions with TmICE less than −10°C (4.9 to 13.4 equiv. wt.% NaCl + $CaCl_2$) (Table 1, Fig. 6).

Type-3 and type-4 inclusions

In some type-3 and type-4 inclusions, no phase changes were observed during the cooling runs; however, in many, a CO_2 melting event was observed (TmCO_2), and in some, clathrate melting (TdCTH) and partial L–V homogenization (ThP) (of the nonaqueous portion of the inclusion) occurred. It is possible that those inclusions that exhibit no phase changes contain very low concentrations of gases other than H_2O; however, their opacity may have obscured any phase changes.

Values of TmCO_2 of type-3 inclusions fall within a narrow range from −59.2 to −58.2°C (Table 2). The only set of type-4 inclusions that yielded data gave a similar value of −59.0°C. Final melting of clathrate ranged from −7 to 8°C, with most values between 5 and 8°C (Table 2). Partial homogenization only was observed in two inclusions, at −1.1 and 4°C, to the vapor phase. In some inclusions, the vapor portion of the CO_2-rich phase was seen to expand on warming from approximately −56°C, but final homogenization could not be seen.

The lowered CO_2 melting point in these inclusions indicates the presence of miscible gases such as CH_4 or N_2, but the lack of reliable data on clathrates or homogenization precludes quantification of their concentrations.

Type-5 inclusions

On cooling type-5 inclusions, the cubic solid generally does not change, and freezing is accompanied by the shrinkage and, in cases, disappearance, of the vapor bubble. On warming, the inclusions appear to start to melt at temperatures ranging from −95 to −60°C, followed by ice melting at temperatures up to approximately −25°C. In most inclusions, after the ice has melted, the cubic
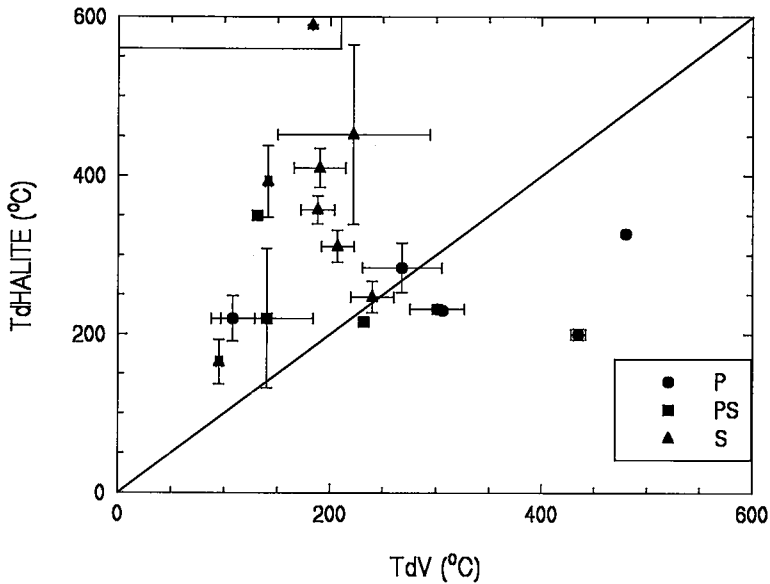
Fig. 7. Temperatures of vapor disappearance (TdV) and halite dissolution
(TdHALITE) for type-5 inclusions. As in Figure 6, points represent averages
and standard deviations.

solid reacts with the liquid, diminishes in size, and a new solid forms around the original solid. In some cases, a new solid is not visible. This reaction indicates that the cubic solid is halite (reacting to form hydrohalite). Where such behavior takes place, ice melting occurs under disequilibrium conditions, as halite is present. In such cases, an equilibrium TmICE was obtained by refreezing the inclusion after the hydrohalite had formed (above the original TmICE value) and before halite had reformed. Subsequent melting of ice was therefore measured in the presence of hydrohalite only. Equilibrium TmICE values range from −54 to −28°C. In some inclusions, no freezing or ice formation was observed, and on warming from less than −100°C, the first event was the reaction of liquid and halite.

On further warming, the hydrohalite melts incongruently to reform halite at temperatures between −0.6 and 23°C (Table 3). Reaction temperatures above 0°C must represent disequilibrium conditions in the inclusions, as hydrohalite is not stable above 0°C (Roedder 1984).

As noted above, those inclusions that contain solids in addition to halite are rare (only observed in a few planes in sample 80–78). The other solids commonly are birefringent, generally anhedral, and have not been identified. Some such inclusions exhibit complex low-temperature behavior; new solids form at the expense of halite and the birefringent solids. Ice was not seen to form in these inclusions.

Average disappearance temperatures of vapor (TdV) and halite (TdHALITE) in type-5 inclusions range from 95 to 480°C (vapor) and from 165 to 452°C (halite) (Fig. 7, Table 3). In most inclusions, TdHALITE was greater than TdV (Fig. 7). Some inclusions decrepitated prior to total homogenization.

The very low TmICE and Te values for type-5 inclusions preclude interpretation of the above data in terms of the $H_2O-NaCl$ or $H_2O-NaCl-KCl$ systems, which have eutectics at −20.8 and −22.9°C, respectively. The dissolved salts are most likely to be a mixture of NaCl, KCl, $CaCl_2$ and $FeCl_2$ (Roedder 1984, Whitney et al. 1985). Given a lack of phase-equilibrium data in $FeCl_2$-bearing systems, we have modeled the composition of type-5 inclusions in terms of the system $H_2O-NaCl-CaCl_2$. The bulk composition of liquid–vapor–halite inclusions in this system may be estimated using TmICE and TdHALITE (Williams-Jones & Samson 1990) (Fig. 8). Type-5 inclusions have modeled salinities of 34 to 52.5 wt.% NaCl + $CaCl_2$ and modeled $NaCl/CaCl_2$ ratios (by weight) of 6.5 to 0.74 (Fig. 8).

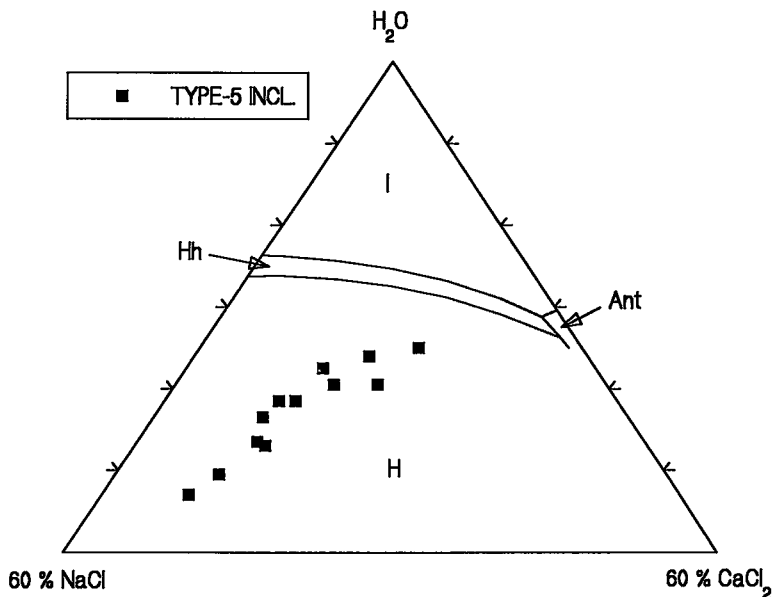FIG. 8. Modeled compositions of type-5 inclusions in the system NaCl–CaCl₂–H₂O. Fields represent composition of aqueous phase in equilibrium with solid indicated. H, halite; I, ice; Hh, hydrohalite; Ant, antarcticite. Phase boundaries from Yanatieva (1946).

Type-6 inclusions

Three minerals are present in type-6 inclusions: 1) tourmaline (rare); 2) muscovite (very common) (Figs. 4B, C, 5B); and 3) a highly birefringent rhombic solid (Fig. 4A).

The muscovite is anhedral to lath-shaped and highly birefringent. The identification of these crystals as muscovite was confirmed with Raman spectroscopy. Muscovite commonly replaces feldspar in the orbicules, and in a few examples appears to be interstitial to the other minerals. The Raman spectra of inclusion solids and of muscovite from the orbicules are shown in Figure 9A. The bands at 100, 260, and 700 cm⁻¹ correspond to those of the muscovite, and agree with published values (Loh 1973). Superimposed on the spectra are the Raman bands for quartz. Quartz and muscovite both have bands at approximately 260 cm⁻¹; however, in the inclusion spectra, the intensity of this band is too high, relative to the other quartz bands, to be attributed only to quartz, which indicates that it is a composite muscovite–quartz band.

The identity of the rhombic mineral has not yet been established. Its optical properties and form suggest that it could be a carbonate; however, the

Raman spectra obtained from this mineral clearly show that it is not (Fig. 9B).

TmICE values were obtained from three type-6 inclusions only (Table 1); they correspond to the TmICE values obtained from the associated type-1 inclusions. On heating, the vapor bubbles in most type-6 inclusions showed no change to temperatures of 50 to 100°C above the homogenization temperatures of associated type-1 inclusions. Some isolated type-6 inclusions in sample 45c, that have no associated type-1 inclusions, and that appear to have consistent ratios of phases, gave TdV values of between 300 and 400°C (Table 1, Fig.6).

DISCUSSION

Nature of the primary fluids

Texturally, the orbicules partly resemble the host granite, which suggests that they in part crystallized from a silicate melt. However, the presence of primary, aqueous, type-1 and type-5 inclusions in quartz, tourmaline and fluorite provides unequivocal evidence that these minerals are partly hydrothermal in origin. This is supported by textural features in the orbicules: tourmaline commonly occurs as a replacement of feldspar and as microveinlets, and fluorite is invariably intersti-
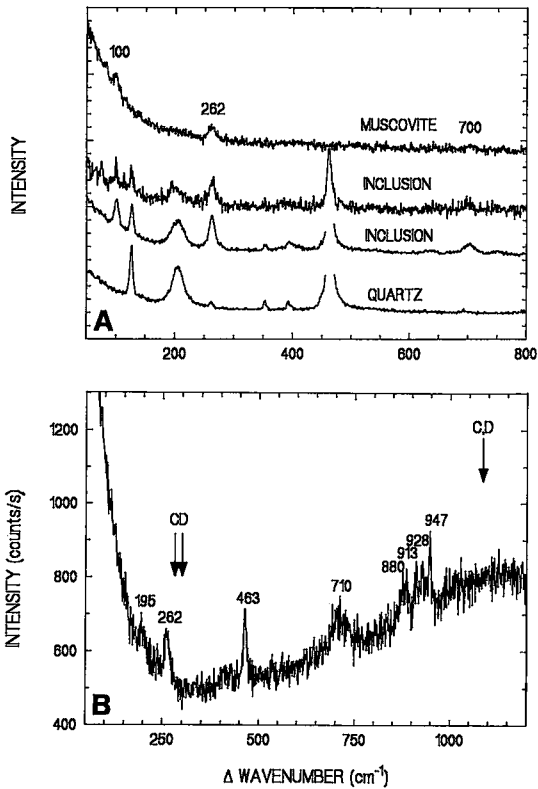
FIG. 10. Ranges of salinity and homogenization temperatures for type-1 and type-5 inclusions.

FIG. 9. A. Raman spectra for muscovite, quartz and two solid inclusions. Peaks at 100, 260, and 700 cm^{-1} are for muscovite; all others pertain to quartz. B. Raman spectrum of rhombic solid inclusion in quartz. Also shown are the principal bands of carbonate minerals, as illustrated by the strongest bands for calcite (C) and dolomite (D).

tial to the other minerals, including quartz, which commonly has bipyramidal terminations. The aqueous fluids responsible for the precipitation of these minerals had salinities ranging from 8 to 42 equiv. wt.% NaCl + CaCl$_2$ (Fig. 10), and are considered to represent orthomagmatic hydrothermal fluids that evolved from the Seagull granitic magma. The lack of tourmaline alteration in the surrounding granite and the general absence of quartz–tourmaline veins extending from the orbicules indicate that the orbicules acted as closed systems during their crystallization and that, in general, the fluids did not escape. The conclusion that the orbicules were closed systems during their crystallization also requires that they in part
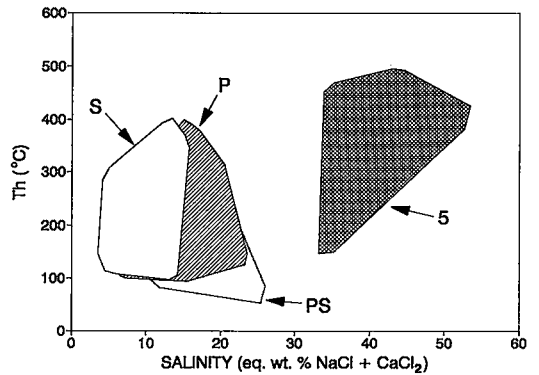
crystallized from a silicate melt, as the required amount of material could not be dissolved in an equivalent volume of hydrothermal fluid.

The presence of muscovite and tourmaline in type-6 inclusions indicates that the hydrothermal fluid was in equilibrium with the assemblage quartz–muscovite–tourmaline, and may therefore be the cause of silicification, tourmalinization or phyllic alteration if it migrated away from its source. The occurrence of quartz–tourmaline veins and the association of phyllic alteration with some of the mineralized veins in the batholith (Mato et al. 1983) indicate that fluids similar to those that were present in the orbicules flowed through the batholith, and may have been responsible for the tin mineralization.

Large variations in the salinity of hydrothermal fluids associated with granitic intrusive bodies have generally been attributed to the involvement and mixing of orthomagmatic and meteoric waters or to boiling. However, recent calculations by Bodnar & Cline (1990) show that the salinity of orthomagmatic fluids generated from a single magma may range from almost pure water to greater than 50 wt.% NaCl, depending on the pressure of crystallization. As the fluid inclusions trapped in the orbicules represent essentially unevolved orthomagmatic fluids, the data collected from the orbicules are consistent with, and support, the calculations of Bodnar & Cline (1990). We cannot rule out boiling as a cause of some of the variations in salinity. Boiling is suggested by, and would explain, the presence of the CO$_2$-rich, type-3 and 4 inclusions; however, they are all secondary, so that their relationship to the other fluids is unknown.

For the type-5 inclusions (mostly from sample 80–78), a positive correlation exists between the

modeled salinities and NaCl/CaCl$_2$ ratios (Fig. 8). There are several possible mechanisms that could cause salinity to covary with NaCl/CaCl$_2$ ratio: differential partitioning of NaCl and CaCl$_2$ between melt and aqueous fluid during exsolution, differential partitioning of these components between liquid and vapor during boiling, mixing of two fluids with different salinities and NaCl/CaCl$_2$ ratios, and halite crystallization.

It is unlikely that the observed trend was produced through mixing, as most of the inclusions that define the trend are from one orbicule. As CaCl$_2$ partitions more strongly than NaCl into the liquid phase during boiling (Zhang & Frantz 1989), this trend could not have been produced through open-system boiling. There are insufficient data on partition coefficients for high-salinity liquids to test a model of closed-system boiling. Because the partition coefficient for CaCl$_2$ between a vapor phase and a granitic melt increases more rapidly with salinity than the coefficient for NaCl (Holland 1972), differential partitioning during crystallization cannot explain the observed trend. The relationship shown on Figure 8 is reminiscent of the halite trend (Cloke & Kesler 1979); however, the extension of the trend on Figure 8 projects to a point on the H$_2$O–NaCl binary, and therefore cannot have been caused by halite crystallization. Further interpretation of the trend on Figure 8 will require more complete compositional data on these inclusions and more data on phase equilibria in the appropriate chemical systems.

P–T conditions of entrapment

As indicated previously, a relatively shallow level of emplacement of the Seagull batholith is inferred from field observations, such as the porphyritic nature of the marginal phases and the presence of miarolitic cavities. The absence of a diagnostic mineral assemblage in the contact aureole precludes a more precise estimate of the P–T conditions. It is likely that the batholith was emplaced at 1 to 2 kbar, or less, which is consistent with the pressure estimate of approximately 1 kbar for emplacement made from stratigraphic reconstructions by Layne & Spooner (1991).

Isochores for primary type-1 and type-5 fluid inclusions are shown in Figure 11. These were calculated using the equation of state of Brown & Lamb (1989) and the computer program FLINCOR (Brown 1989). For isochore calculations, the inclusions have been modeled on the system H$_2$O–NaCl, as CaCl$_2$ contents are not known for the type-1 inclusions. By ignoring CaCl$_2$, the calculated isochore for a given Th will be slightly shallower than if CaCl$_2$ were included (Zhang & Frantz 1987). Primary inclusions have a wide range
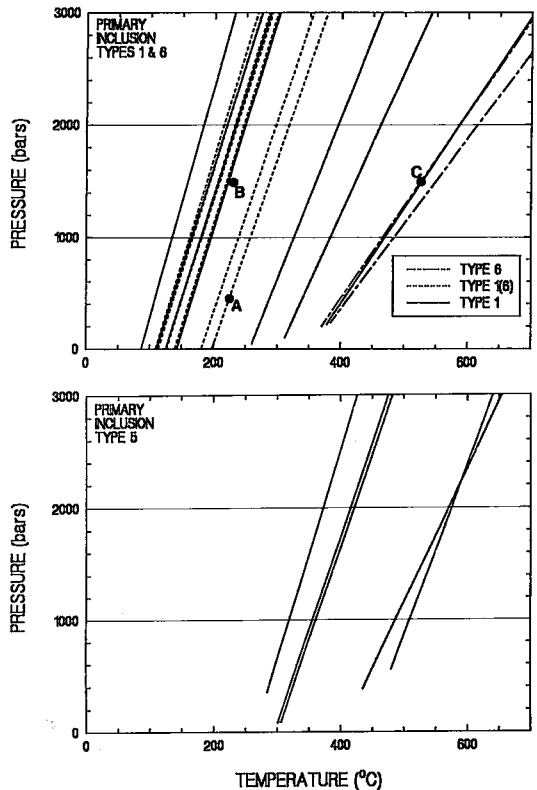

FIG. 11. Isochores for primary inclusions of types 1, 5 and 6. Horizontal lines at 1 and 2 kbar represent likely minimum and maximum pressures of entrapment. Points A, B and C are discussed in the text.

of homogenization temperatures, from approximately 100 to 500°C (Figs. 6, 10). With trapping pressures of 1 to 2 kbar, the highest-temperature inclusions will have been trapped at or close to liquidus temperatures (500 to 600°C) (Fig. 11), given that late-stage granitic melts may exist at temperatures as low as 450 to 500°C (Manning 1981, Manning & Pichavant 1984, London 1989). Those inclusions that homogenized at lower temperatures must have either cooled significantly prior to entrapment, in some cases down to around 150°C, or their densities have been increased subsequent to entrapment. As there appears to have been little fluid leakage out of the orbicules, it is reasonable to hypothesize that crystallization occurred over a protracted period and, therefore, that the fluids may have cooled significantly before precipitating some of the quartz and tourmaline. However, the type-1 inclusions that are associated

with type-6 inclusions all have low Th values (Figs. 6, 11). As these inclusions are commonly associated with type-2 inclusions, and with a type-6 inclusion that commonly contains a large vapor bubble, it is quite likely that these arrays formed at moderately high temperatures, but underwent necking during subsequent cooling. The necking-off of a large vapor bubble attached to the solid (Fig. 5) would result in an increase in the density of the subsequently formed inclusions, resulting in low temperatures of homogenization. This also explains the presence of type-2 inclusions in these clusters. In support of this model, the isolated type-6 inclusions (no type-1 inclusions) that were homogenized indicate entrapment conditions of 500 to 600°C (Fig. 11).

The density of fluid inclusions may also be increased through re-equilibration during cooling. This occurs where the external pressure greatly exceeds the pressure within the fluid inclusion (as constrained by the original isochore for the inclusion), as would occur during isobaric cooling (Sterner & Bodnar 1989). This pressure differential generally results in the formation of an implosion halo of new fluid inclusions around the original inclusion (Sterner & Bodnar 1989). Although some of the 6/1 arrays resemble the textures described by Sterner & Bodnar, and it is possible that the Seagull batholith cooled nearly isobarically, the generally planar nature of the 6/1 arrays suggests that most did not form in this manner.

The low temperatures of homogenization for the 6/1 arrays are further evidence that they are not decrepitation-induced clusters. Decrepitation results in a decrease in fluid density and, therefore, an increase in Th. In order to obtain the fluid densities for the type-1 inclusions in these arrays (e.g., point A, Fig. 11), the original inclusions must have been trapped at temperatures of less than 200 to 230°C (point B, Fig. 11), assuming that a minimum overpressure of 1 kbar is required for decrepitation. In order also to explain the higher-temperature primary inclusions (e.g., point C, Fig. 11), the uplift path for the batholith would require almost isobaric cooling (C → B), followed by almost isothermal decompression (B → A). Such a path of uplift is highly unlikely.

CONCLUSIONS

The quartz–tourmaline orbicules that occur in the roof zone of the Seagull batholith represent a transition from magmatic to hydrothermal processes. The orbicules crystallized from residual bubbles of a mixture of borosilicate melt and orthomagmatic hydrothermal fluid that formed in a largely crystallized granitic magma. This explains the rounded form of the orbicules. High degrees

of crystallization were probably required to produce a Si-rich residue with the high viscosities necessary to prevent coalescence and migration of the melt–fluid mixture.

A significant proportion of the quartz and probably all of the tourmaline and fluorite in the orbicules was precipitated from unevolved orthomagmatic hydrothermal fluids with salinities that ranged from 8 to 42 equiv. wt.% NaCl + $CaCl_2$. As the orbicules crystallized as closed systems, these values suggest that large ranges in salinity of the hydrothermal fluids associated with granitic intrusive bodies may represent original variations in the exsolved fluid rather than variations that resulted from boiling or mixing with a meteoric fluid.

Isochoric projections indicate that hydrothermal precipitation probably occurred between 600 and 300°C, and possibly as low as 150°C.

The hydrothermal fluid that precipitated the quartz in the orbicules was in equilibrium with muscovite, rather than K-feldspar. Therefore, the migration of these fluids through the granite would initially cause phyllic alteration.

Elevated concentrations of tin in the orbicules, relative to the surrounding granite, indicate that tin was concentrated in these residual melts and possibly in the orthomagmatic hydrothermal fluids. Quartz–tourmaline veins in the Seagull batholith and its country rocks are evidence that fluids similar to those that formed the orbicules escaped from the crystallizing melt, and were likely responsible for the tin mineralization around the Seagull batholith. However, information on the character of fluids responsible for the vein systems and for the tin mineralization is required to chart the evolution of the magmatic fluids and to test this hypothesis.

REFERENCES

ABBOTT, J.G. (1981): Geology of Seagull tin district. In Yukon Geology and Exploration 1979-1980. Dep. Indian Affairs and Northern Development, 32-44.

BODNAR, R.J. & CLINE, J.S. (1990): Microthermometric and phase behaviour of magmatic–hydrothermal fluid inclusions: an analysis based on PVTX data for the system albite-H_2O-NaCl. Third PACROFI Conf. (Toronto), Program Abstr., 17.

BROWN, P.E. (1989): FLINCOR: a microcomputer

program for the reduction and investigation of fluid-inclusion data. *Am. Mineral.* **74**, 1390-1393.

———— & LAMB, W.M. (1989): P–V–T properties of fluids in the system $H_2O \pm CO_2 \pm NaCl$: new graphical presentations and implications for fluid inclusion studies. *Geochim. Cosmochim. Acta* **53**, 1209-1221.

CLOKE, P.L. & KESLER, S.E. (1979): The halite trend in hydrothermal solutions. *Econ. Geol.* **74**, 1823-1831.

DICK, L.A. (1980): *A Comparative Study of the Geology, Mineralogy, and Conditions of Formation of Contact Metasomatic Mineral Deposits in the Northeastern Canadian Cordillera.* Ph.D. thesis, Queen's Univ., Kingston, Ontario.

GOWER, J.A. (1952): *The Seagull Creek Batholith and its Metamorphic Aureole.* M.A.Sc thesis, Univ. British Columbia, Vancouver, British Columbia.

GRATIER, J.P. & JENATTON, L. (1984): Deformation by solution-deposition, and re-equilibration of fluid inclusions in crystals depending on temperature, internal pressure and stress. *J. Struct. Geol.* **6**, 189-200.

HOLLAND, H.D. (1972): Granites, solutions and base metal deposits. *Econ. Geol.* **67**, 281-301.

LAYNE, G.D. & SPOONER, E.T.C. (1986): The JC Sn–Fe–F skarn, Seagull Batholith area, southern Yukon. *In* Mineral Deposits of the Northern Cordillera (J.A. Morin, ed.). *Can. Inst. Min. Metall., Spec. Pap.* **37**, 266-273.

———— & ———— (1991): The JC tin skarn deposit, southern Yukon Territory. I. Geology, paragenesis, and fluid inclusion microthermometry. *Econ. Geol.* **86**, 29-47.

LOH, E. (1973): Optical vibrations in sheet silicates. *J. Phys. C.: Solid State Phys.* **6**, 1091-1104.

LONDON, D. (1989): Lithophile rare element concentration in peraluminous silicate systems: summary of experimental results with Macusani glass. *Geol. Assoc. Canada – Mineral. Assoc. Can., Program Abstr.* **14**, A32.

MANNING, D.A.C. (1981): The effect of fluorine on liquidus phase relationships in the system Qz–Ab–Or with excess water at 1 kb. *Contrib. Mineral. Petrol.* **76**, 206-215.

———— & PICHAVANT, M. (1984): Experimental studies of the role of fluorine and boron in the formation of late-stage granitic rocks and associated mineralization. *Proc. 27th Int. Geol. Congress (Moscow)* **9**, 353-372.

MATO, G., DITSON, G. & GODWIN, C. (1983): Geology and geochronometry of tin mineralization associated with the Seagull batholith, south-central Yukon

Territory. *Can. Inst. Min. Metall., Bull.* **76**(854), 43-49.

OAKES, C.S., BODNAR, R.J. & SIMONSON, J.M. (1990): The system $NaCl–CaCl_2–H_2O$. I. The ice liquidus at 1 atm total pressure. *Geochim. Cosmochim. Acta* **54**, 603-610.

PÉCHER, A. (1981): Experimental decrepitation and re-equilibration of fluid inclusions in synthetic quartz. *Tectonophys.* **78**, 567-583.

POOLE, W.H. (1956): *Geology of the Cassiar Mountains in the Vicinity of the Yukon – British Columbia Boundary.* Ph.D. thesis, Princeton Univ., Princeton, New Jersey.

ROEDDER, E. (1984): Fluid inclusions (P.H. Ribbe, ed.). *Rev. Mineral.* **12**.

SINCLAIR, W.D. (1986): Molybdenum, tungsten and tin deposits and associated granitoid intrusions in the northern Canadian Cordillera and adjacent parts of Alaska. *In* Mineral Deposits of Northern Cordillera (J.A. Morin, ed.). *Can. Inst. Min. Metall., Spec. Pap.* **37**, 216-233.

———— & RICHARDSON, J.M. (1992): Quartz–tourmaline orbicules in the Seagull batholith, Yukon Territory. *Can. Mineral.* **30**, 923-935.

STERNER, S.M. & BODNAR, R.J. (1989): Synthetic fluid inclusions. VII. Re-equilibration of fluid inclusions in quartz during laboratory-simulated metamorphic burial and uplift. *J. Metamorph. Geol.* **7**, 243-260.

TEMPELMAN-KLUIT, D.J. (1979): Transported cataclasite, ophiolite, and granodiorite in Yukon: evidence of arc–continent collision. *Geol. Surv. Can., Pap.* **79-14**.

TISCHENDORF, G. (1977): Geochemical and petrographic characteristics of silicic magmatic rocks associated with rare-element mineralization. *In* Metallization Associated with Acid Magmatism 2 (M. Stemprok, L. Burnol & G. Tischendorf, eds.). Geol. Surv. Czechoslovakia, Prague (41-96).

WHITNEY, J.A., HEMLEY, J.J. & SIMON, F.O. (1985): The concentration of iron chloride solutions equilibrated with synthetic granite compositions: the sulfur-free system. *Econ. Geol.* **80**, 444-460.

WILLIAMS-JONES, A.E. & SAMSON, I.M. (1990): Theoretical calculations of halite solubility in the system $NaCl–CaCl_2–H_2O$: applications to fluid inclusions. *Can. Mineral.* **28**, 299-304.

YANATIEVA, O.K. (1946): Polythermal solubilities in the systems $CaCl_2–MgCl_2–H_2O$ and $CaCl_2–NaCl–H_2O$. *Zh. Prikl. Khim.* **19**, 709-722 (in Russ.).

ZHANG YI-GANG & FRANTZ, J.D. (1987): Determination of the homogenization temperatures and densities of supercritical fluids in the system $NaCl–KCl–CaCl_2–$

H_2O using synthetic fluid inclusions. *Chem. Geol.* **64**, 335-350.

‗‗‗‗ & ‗‗‗‗ (1989): Experimental determination of the compositional limits of immiscibility in the system $CaCl_2$–H_2O–CO_2 at high temperatures and pressures using synthetic fluid inclusions. *Chem. Geol.* **74**, 289-308.